Preparation, Characterization, and Catalytic Performance of Bismuth−Aluminum Binary-Oxide Layers and Clusters on an Al_2O_3 Surface

T. Shido,[†] G. Okita,[†] K. Asakura,[†,‡] and Y. Iwasawa*[,†]

Department of Chemistry, Graduate School of Science, the University of Tokyo, Hongo, Bunkyo-ku, Tokyo 113-0033, Japan

Received: June 16, 2000

Bismuth−aluminum binary-oxide layers and clusters on an Al_2O_3 surface were prepared by supporting bismuth triethoxides on Al_2O_3, followed by calcination at 673 K. The Bi−Al binary oxides were characterized by EXAFS and XPS, and their catalytic activities for ethanol-selective oxidation were investigated. XPS data revealed that Bi atoms were supported on the Al_2O_3 surface in a Stranski−Krastanov (SK) growth mode, while EXAFS data demonstrated that Bi atoms made bondings with Al atoms at 0.353−0.361 nm through oxygen atoms (Bi−O, 0.211−0.212 nm) irrespective of Bi loadings and that the coordination numbers (CN) of the Bi−Al bond did not significantly change with Bi loadings (CN, 1.0−1.5). It is likely from these results that below 9 wt % Bi loading, Bi−Al (rich) binary-oxide monolayers are formed at the Al_2O_3 surface and that above 9 wt % Bi loading, Bi (rich)−Al binary-oxide clusters grow on the surface. In the low-Bi-loading catalysts, Bi−O and Bi−Al bonds were observed at 0.211 and 0.353−0.355 nm, respectively, while no Bi−Bi bond was observed, which suggests that Bi atoms are dispersed in the oxide layers. On the other hand, in the high-Bi-loading catalysts, Bi−Bi and long Bi−O bonds were observed at 0.363−0.369 and 0.276−0.279 nm, respectively, in addition to Bi−O at 0.212 nm and Bi−Al at 0.359−0.361 nm. The distances of the long Bi−O and Bi−Bi bonds were comparable to their distances in γ-Bi_2O_3, and the Bi−Al distance was also close to that in bismuth binary oxides with the γ-Bi_2O_3 phase. These results suggest that the Bi (rich)−Al binary-oxide clusters have a γ-Bi_2O_3-like structure. The catalytic activity of these binary oxides at the Al_2O_3 surface for ethanol-selective oxidation strongly depended on the structure around bismuth atoms. The initial rate for acetaldehyde formation steeply increased around 9 wt % Bi loading. The activation energy for the 11.0 wt % Bi/Al_2O_3 catalyst was 53 kJ mol^{-1}, while that for the 7.6 wt % Bi/Al_2O_3 catalyst was 96 kJ mol^{-1}, reflecting the different local structure of the active Bi sites.

1. Introduction

Metal oxides dispersed on high-surface-area supports are one of the most promising families of catalysts in the effective use of resources. In these systems, control of the structure and bond arrangement of the surface are the keys to generating good catalytic performances, which may lead to the development of new catalytic materials and systems.[1−10] Supporting metal complexes/clusters on robust oxide surfaces, followed by chemical treatments in a controllable manner, has a great advantage to preparing dispersed active species with uniform character, compared to conventional wet impregnation and dry sublimation methods using metal salts. This kind of catalyst can be characterized by sophisticated physical techniques on a molecular scale.[1−4] Using this method, we have prepared monolayer catalysts of Ti,[11−13] V,[14−18] Cr,[19,20] Mn,[21] Ni,[22] Cu,[23] Zr,[24] Nb,[25,26] and W[27,28] to examine their performances for partial oxidation reactions.

Bismuth is an important element in catalysis. It is a key element of selective oxidation catalysts such as bismuth molybdates.[29−33] Yttria-doped bismuth oxide is one of the most active catalysts for oxidative coupling of methane.[34]

Highly crystalline bismuth oxides are often employed to obtain good performance for selective oxidation, which utilizes the bulk oxygen atoms. In contrast to this aspect of catalysis, the catalytic property of high-surface-area crystalline bismuth oxide clusters/particles dispersed on oxide-support surfaces may be of interest from the viewpoints of catalytic chemistry and surface science to developing new subnanosize to nanosized surface catalytic materials.

In this paper, we have prepared bismuth oxides on Al_2O_3 using $Bi(OEt)_3$ as a precursor and changing the Bi loading systematically and characterized the obtained samples by extended X-ray absorption fine structure (EXAFS) and X-ray photoelectron spectroscopy (XPS). It was found that bismuth−aluminum (rich) binary oxide layers below 9 wt % Bi loading and bismuth (rich)−aluminum clusters above 9 wt % Bi loading were formed at the Al_2O_3 surface, which were almost inactive and active, respectively, for the selective catalytic oxidaition of ethanol to acetaldehyde.

2. Experimental Section

Al_2O_3-supported bismuth oxide catalysts were prepared by an impregnation method using an ethanol solution of given amounts of $Bi(OEt)_3$ which was synthesized from $BiCl_3$.[35] The alumina (Aerosil, Al_2O_3−C) was pre-evacuated at 573 K in situ before interacting with the $Bi(OEt)_3$ solution. The obtained suspension of Al_2O_3 in the solution was stirred at room

* Corresponding author. Fax: +81-3-5800-6892. E-mail: iwasawa@chem.s.u-tokyo.ac.jp.
[†] University of Tokyo.
[‡] Present address: Catalysis Research Center, Hokkaido University, Kita-ku, Sapporo 060-0811, Japan.

10.1021/jp0021650 CCC: $19.00
Published on Web 12/02/2000

temperature for 2 h, followed by evaporation of the solvent in a vacuum. The dried sample was calcined at 673 K for 2 h in an oxygen flow. The bismuth loading was regulated in the range 0.5−36 wt %, which was determined by ICP.

XPS spectra were recorded on a Shimadzu XPS-7000 ESCA apparatus at a base pressure of 1×10^{-7} Pa. The X-ray source, voltage, and current were Mg Kα, 10 kV, and 20 mA, respectively. The binding energies were calibrated using Al 2p.

EXAFS spectra at Bi L_{III}-edge were measured in transmission mode at 10 K at BL-10B station of the Photon Factory in the Institute of Materials Structure Science, High Energy Accelerator Research Organization (KEK−IMSS−PF). The energy and current of electrons in the storage ring were 2.5 GeV and 200−300 mA, respectively. X-rays from the storage ring were monochromatized by a Si(311) channel cut crystal. Ionization chambers filled with pure N_2 and Ar/N_2 (15:85) mixed gas were used to monitor the incident and transmitted X-rays, respectively. The samples for EXAFS measurements were prepared in a way similar to that described in the catalyst preparation. The samples were transferred to EXAFS cells with Kapton windows without exposure to air. To minimize the effect of higher harmonics, we regulated the sample thickness so that the total absorbance was less than 3. The EXAFS spectra were analyzed by the UWXAFS package.[36] The threshold energy E_0 was tentatively set at the inflection point of the absorption edge. The background was subtracted by the AUTOBK program. The k^3-weighted EXAFS data were Fourier transformed into R-space. The curve-fitting analysis was carried out using the FEFFIT program in the R-space. The k-range for the Fourier transformation and the fitting R-range were 30−110 nm^{-1} and 0.1−0.4 nm, respectively. The number of independent parameters (N_{idp}) in the curve-fitting was evaluated to be 17 from the Niquest law[37]

$$N_{idp} = \frac{2\Delta k \Delta R}{\pi} + 2$$

The fitting parameters were coordination numbers (CN), interatomic distances (R), Debye−Waller factors (σ), and a correction-of-edge energy (ΔE_0). The same ΔE_0 was used for all the shells in a sample. The Bi/Al_2O_3 samples with Bi loadings less than 7.6 wt % (low-loading samples) were fitted by two shells, Bi−O and Bi−Al, whereas the samples whose Bi loadings were larger than 10.0 wt % (high-loading samples) were fitted by four shells, two Bi−O's, one Bi−Al, and one Bi−Bi. Hence, the numbers of fitting parameters for low- and high-loading samples are seven and thirteen, respectively, which are smaller than the N_{idp}. The phase shift and the backscattering amplitude for Bi−O, Bi−Al, and Bi−Bi bonds were calculated by the FEFF8 code.[38]

The coefficient of the multiphoton effect (S_0^2) was estimated to be 0.5 by the comparison of the first shell (Bi−O) between observed and simulated EXAFS functions of Bi_2O_3. The crystallographic data for α-Bi_2O_3[39] was used to calculate the spectrum.

The ethanol partial oxidation reaction was carried out in a closed circulating reactor system whose base pressure and dead volume were 10^{-3} Pa and 220 cm^3, respectively. The catalyst amounts, reaction temperatures, and ethanol and oxygen pressures were 30−200 mg, 393−473 K, 2.7 kPa, and 3.4 kPa, respectively. Reaction products were analyzed by a gas chromatograph using Unibeads C and Porapack-P columns. Unibeads C were used to separate CO and CO_2, while Porapack-P was used for the analysis of ethanol, dietyl ether, acetic acid, and ethene.

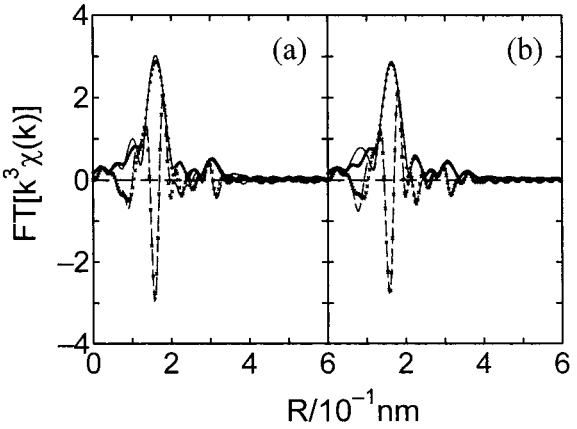

Figure 1. Fourier transformed k^3-weighted EXAFS functions for the Bi/Al_2O_3 catalysts: (a) 4.7 wt % Bi and (b) 11.0 wt % Bi. Solid lines, dashed lines, (●●●), and (×××) represent the absolute values of the observed data, the imaginary parts of the observed data, the absolute values of the calculated spectra, and the imaginary parts of the calculated spectra, respectively.

Temperature-programmed desorption (TPD) of adsorbed ethanol was carried out using a glass-made vacuum line. Before the TPD experiment, the sample was exposed to 2.7 kPa of ethanol for 15 min at room temperature, followed by evacuation for 30 min. The heating rate was 5 K/min^{-1}.

3. Results and Discussion

3.1. Characterization of Bi/Al_2O_3. Figure 1 shows Fourier-transformed EXAFS functions ($k^3\chi(k)$) and their curve-fitting results for Bi/Al_2O_3 catalysts (4.7 and 11.0 wt %). The phase shift was not corrected in these spectra. A large peak was observed at 0.17 nm, and small peaks were observed at 0.22, 0.28, 0.31, and 0.36 nm. The observed spectra were reproduced well by the theoretical calculation. The fact that no peak was observed above 0.4 nm demonstrates the high signal-to-noise ratio of the spectra, and hence, the four small peaks in 0.2−0.4 nm may have physical meaning. The shapes of the four peaks for the low-Bi-loading catalysts (4.7 and 7.6 wt %) and the high-Bi-loading catalysts (10.0, 11.0, and 27.0 wt %) were slightly different from each other, as shown in Figure 2 (uncorrected for the phase shift). In the low-loading catalysts, the four peaks were somehow broad and overlapped with each other. The peak at 0.36 nm was especially tbroad. On the other hand, these small peaks for the high-Bi-loading catalysts were well resolved. The shape of the imaginary part for each shell in Figure 2 was basically the same in all the catalysts, which implies that the origin (the absorber−scatterer pairs) for each of the four peaks could be the same in those catalysts.

Table 1 shows structural parameters derived by the curve-fitting analysis. The Fourier-transformed EXAFS functions for the high-Bi-loading catalysts (10.0, 11.0, and 27.0 wt %) were fitted by the four shells, Bi−O, Bi−O, Bi−Al, and Bi−Bi. For the low-Bi-loading catalysts (4.7 and 7.6 wt %), longer Bi−O and Bi−Bi bonds were not included because the residual factors did not decrease by the inclusion of these shells and because the calculated structural parameters were not reasonable. In the case of high-Bi-loading catalysts, the residual factor decreased substantially by adding Bi−O around 0.28 nm and Bi−Bi around 0.36 nm, and the calculated structural parameters were reasonable, as shown in Table 1.

The error bars in the parameters for the nearest Bi−O bonds are small. The error bars in the parameters for Bi−Al, the second nearest Bi−O, and Bi−Bi bondings are relatively large because

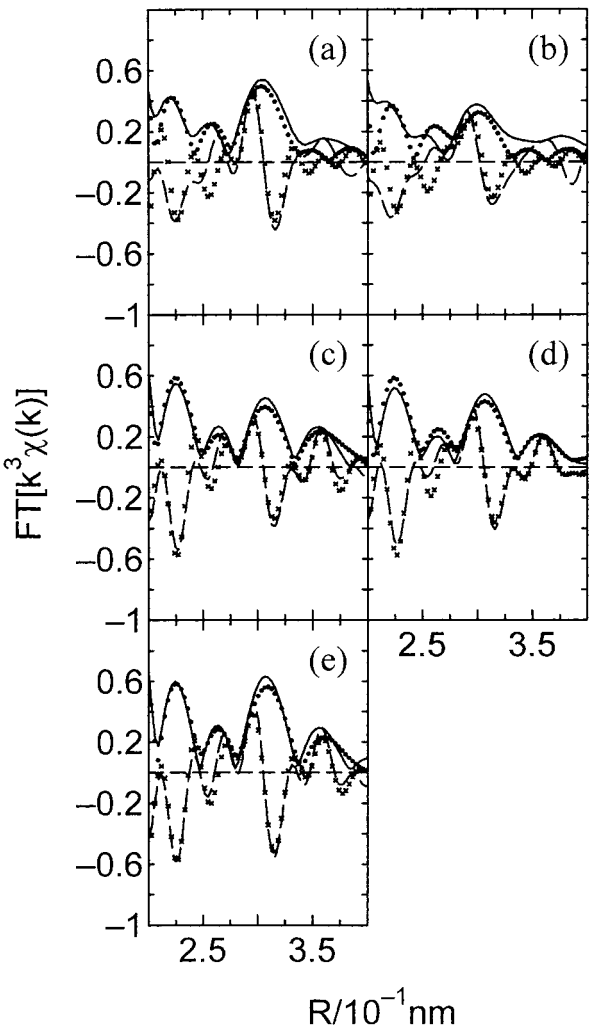

Figure 2. Fourier transformed k^3-weighted EXAFS functions for the Bi/Al_2O_3 catalysts. Bi loadings: (a) 4.7, (b) 7.6 (c) 10.0, (d) 11.0, and (e) 27.0 wt %. Solid lines, dashed lines, (●●●), and (×××) represent the absolute values of the observed data, the imaginary parts of the observed data, the absolute values of the calculated spectra, and the imaginary parts of the calculated spectra, respectively.

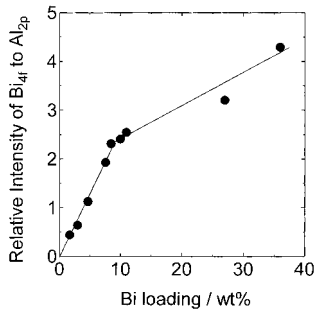

Figure 3. XPS peak intensity of Bi 4f (7/2 + 5/2) relative to the Al 2p peak intensity as a function of Bi loading.

the contribution to the EXAFS functions is small and these shells are overlapping. Especially since the CN and Debye−Waller factor correlate strongly with each other, the CN cannot be obtained accurately. The CN and the distance of the nearest Bi−O bond were independent of the Bi loading and were 4.0 ± 0.3 and 0.211 ± 0.001 nm, respectively. Furthermore, the CN and the distance of Bi−Al bond were observed in the ranges 1.0−1.5 and 0.353−0.361 nm, respectively, for all the catalysts. The change in the values was not so with different Bi loadings. The results might indicate that bismuth oxide species grow to monolayers without changing in the Bi−Al interfacial bonding feature at the Al2O3 surface. But this is not the case for the Bi/Al_2O_3 catalysts, as discussed hereafter.

TABLE 1: Curve-Fitting Results for the Bi/Al_2O_3 Catalysts

catalyst and shell	CN	R/(0.1nm)	$\sigma/10^{-4}$ (nm)	ΔE_0 (eV)	R_f (%)
		Bi/Al_2O_3 (Bi 4.7 wt %)			
Bi−O	4.1 ± 0.4	2.11 ± 0.01	5.5 ± 1.0	−1.2 ± 2.0	4.1
Bi−Al	1.2 ± 0.9	3.56 ± 0.02	7 ± 5		
		Bi/Al_2O_3 (Bi 7.6 wt %)			
Bi−O	4.2 ± 0.3	2.11 ± 0.01	6.8 ± 1.0	−1.4 ± 1.7	3.8
Bi−Al	1.1 ± 1.1	3.53 ± 0.05	12 ± 11		
		Bi/Al_2O_3 (Bi 10.0 wt %)			
Bi−O	3.9 ± 0.3	2.12 ± 0.01	5.5 ± 0.9	−0.4 ± 2.0	2.2
Bi−O	1.3 ± 0.5	2.77 ± 0.06	14 ± 4		
Bi−Al	1.0 ± 0.8	3.59 ± 0.05	6 ± 8		
Bi−Bi	1.8 ± 1.0	3.63 ± 0.06	12 ± 5		
		Bi/Al_2O_3 (Bi 11.0 wt %)			
Bi−O	3.8 ± 0.3	2.12 ± 0.01	5.1 ± 0.9	−0.3 ± 1.7	2.2
Bi−O	0.8 ± 0.4	2.79 ± 0.07	10 ± 5		
Bi−Al	1.4 ± 0.8	3.61 ± 0.07	13 ± 6		
Bi−Bi	2.3 ± 1.6	3.69 ± 0.08	19 ± 8		
		Bi/Al_2O_3 (Bi 27.0 wt %)			
Bi−O	4.2 ± 0.3	2.12 ± 0.01	5.3 ± 0.7	1.0 ± 2.0	0.9
Bi−O	0.8 ± 0.6	2.76 ± 0.06	11 ± 6		
Bi−Al	1.5 ± 0.8	3.60 ± 0.03	7 ± 5		
Bi−Bi	2.7 ± 2.0	3.66 ± 0.05	16 ± 8		

The Bi−Bi distances in the high-loading catalysts were not affected by an increase of the Bi loading, whereas the Bi−Bi CNs increased a little with increasing Bi loading. In addition to the Bi−Bi bonds, longer Bi−O bonds at 0.276−0.279 nm were observed with high-Bi-loading catalysts (10.0, 11.0, and 27.0 wt %), as shown in Table 1. The longer Bi−O and Bi−Bi bonds were not observed with low-Bi-loading catalysts (4.7 and 7.6 wt %), but it does not mean straightforwardly that the bismuth species in low-loading catalysts are isolatedly dispersed on the Al_2O_3 surface because EXAFS oscillations are often smeared when interatomic distances are heterogeneously distributed. As the structural parameters for the nearest Bi−O and Bi−Al bonds and the shape of the Fourier-transformed EXAFS functions in the high- and low-Bi-loading catalysts are similar to each other, the bond arrangement of Bi−O−Al at the Al_2O_3 surface in the high- and low-Bi-loading catalysts may be similar.

The observation of the Bi−Bi and longer Bi−O bonds at definite distances with CNs of 1.8−2.7 and 0.8−1.3, respectively, indicates that the bismuth oxide species in the high-loading catalysts (≥10 wt %) have an ordered structure rather than an amorphous phase. The Bi−Bi distances of the Bi/Al_2O_3 catalysts (0.363−0.369 nm) are comparable to those for α- and γ-Bi_2O_3. In addition, the Bi−O bonds at 0.276−0.279 nm also exist in the crystals of α- and γ-Bi_2O_3.[39,40] Thus, the structure of the bismuth oxide species in the high-loading catalysts seems to be close to the part of bulk Bi_2O_3.

Figure 3 shows the intensity of Bi 4f (5/2 + 7/2) XPS peaks relative to that of Al 2p XPS peak as a function of Bi loading. Up to 8.5 wt %, the relative intensity was proportional to the loading. There was a break at 9 wt % followed by a gentle slope with increasing Bi loading. The results demonstrate that the morphology and/or state of the supported bismuth oxides changes at the Bi loading of 9 wt %. Figure 3 looks a Stranski−Krastanov (SK) growth mode, where the bismuth oxide monolayer is completed at 9 wt % and bismuth oxide clusters/particles are deposited on the monolayer. However, the break point is much lower than the Bi quantity for the bismuth oxide monolayer, which is estimated to be 27−34 wt %.

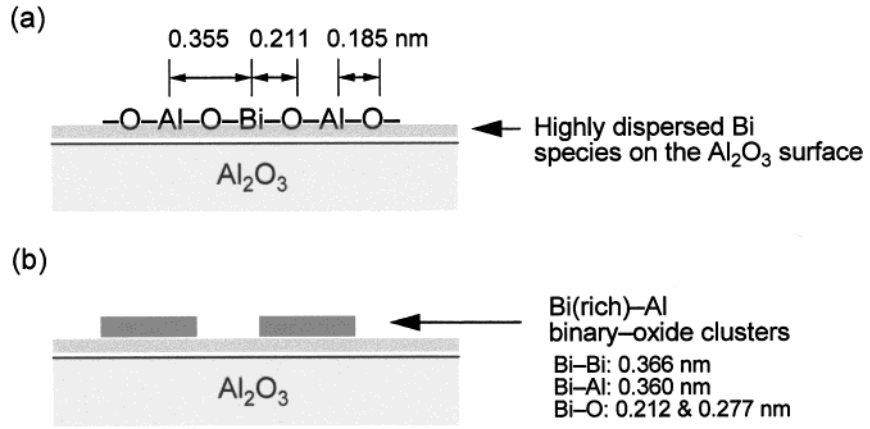

Figure 4. Proposed structures of bismuth oxide species on an surface. (a) Bi loading, <7.6 wt %. (b) Bi loading, ≥10 wt %.

The curve-fitting results in Table 1 also indicate that the reality is more complicated. If the SK growth model is the case, the CN of Bi−Bi in Bi/Al_2O_3 (27.0 wt %) should be larger, and the CN of Bi−Al should be smaller compared to the observed values because the bismuth oxide clusters/particles have lots of Bi−Bi bonds but no Bi−Al bonds in the clusters/perticles. The discussion would be valid also in the case of the Frank−van der Merwe (FM) layer-by-layer growth mode.

We propose from the EXAFS data that Bi−Al binary oxides were formed on the Al_2O_3 surface. It has been reported that Bi forms binary oxides with Al, Si, Fe, Zr, Ce, Tl, and Pb, and these binary oxides have a γ-Bi_2O_3 structure.[40] In the bulk Bi−M binary oxides, the Bi−Bi and Bi−M distances are 0.36−0.37 and 0.35−0.37 nm, respectively. The observed Bi−Bi and Bi−Al distances in the Bi/Al_2O_3 catalysts are 0.363−0.369 and 0.353−0.361 nm, respectively, which are similar to those for γ-Bi_2O_3 crystal-based binary oxides. In addition, observation of longer Bi−O bonds at 0.276−0.279 nm also supports the proposition because they correspond to the Bi−O bonds at 0.26−0.29 nm in the crystal. For the low-Bi-loading catalysts, the Bi−Al bond was observed, whereas the Bi−Bi bond was not observed. When Bi−Bi distances are widely distributed in a complex manner, the Bi−Bi bond is hardly detected by EXAFS. It is more plausible that Bi ions are highly dispersed at the Al_2O_3 surface because the Bi loadings before the break in Figure 3 are much smaller than the Bi_2O_3 monolayer.

The combined results of EXAFS and XPS reveal that the bismuth oxide species at the Al_2O_3 surface form a Bi−Al binary oxide phase. In the range of Bi loading <9 wt %, the domain of the Bi−Al (rich) binary oxide layer at the Al_2O_3 surface increases with an increase in Bi loading. After the break at 9 wt %, Bi (rich)−Al binary-oxide clusters are formed on the Bi−Al (rich) binary-oxide layer. The Bi (rich)−Al binary oxide with γ-Bi_2O_3 structure may have a component of $Bi_{12}AlO_{20}$.[40] The highly dispersed Bi species can probably be stabilized only in the low Bi loading, and above the critical Bi quantity (9 wt %), three-dimensional Bi (rich)−Al binary-oxide clusters may be preferable. As the error bar in the Bi−Bi coordination number is large and the Bi−Bi bonding in bulk γ-Bi_2O_3 is complicated, the exact cluster size cannot be obtained from the EXAFS data. The cluster size should not be so large, however, because no peak was observed in the distance longer than 0.4 nm (Figure 1) and because no X-ray diffraction pattern was observed.

Figure 4 shows proposed structures of bismuth oxides supported at the Al_2O_3 surface. Below 9 wt % Bi loading, the bismuth ions are highly dispersed to form the surface Bi−Al (rich) binary-oxide layers. Above 9 wt %, the Bi (rich)−Al binary-oxide clusters grow on the surface. The proposed structures can explain both EXAFS and XPS data.

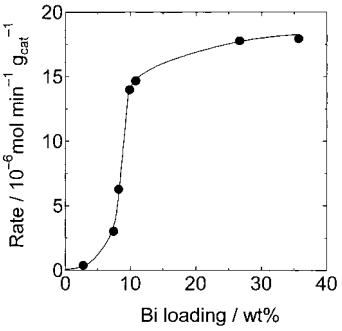

Figure 5. Initial rates for acetaldehyde formation at 433 K as a function of Bi loading in the attached Bi/Al_2O_3 catalysts. $P_{C_2H_5OH}$: 2.66 kPa; P_{O_2}: 3.35 kPa.

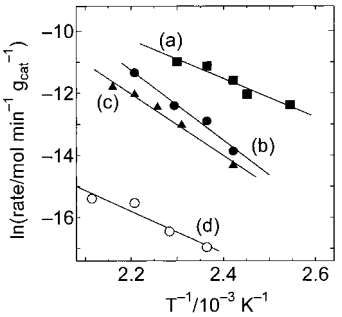

Figure 6. Arrhenius plots for ethanol oxidation on (a) Bi/Al_2O_3 (11.0 wt %), (b) Bi/Al_2O_3 (7.6 wt %), (c) impregnated Bi/Al_2O_3 (10 wt %), and (d) Bi_2O_3. The activation energies for a−d are 53 ± 8, 96 ± 10, 84 ± 7, and 57 ± 12, respectively.

3.2. Ethanol Selective Oxidation. It was found that the Bi/Al_2O_3 catalysts were active for ethanol-selective oxidation to produce acetaldehyde. Figure 5 shows the initial rates of acetaldehyde formation as a function of Bi loading. The catalytic activity of the 3 wt % Bi/Al_2O_3 catalyst was negligible. The activity increased very steeply when the Bi loading was close to 10 wt %. Above 10 wt %, the activity of the Bi/Al_2O_3 catalysts was almost unchanged with Bi loading.

Figure 6 shows Arrhenius plots for acetaldehyde formation on a supported Bi/Al_2O_3 catalyst, an impregnated Bi/Al_2O_3 catalyst, and bulk Bi_2O_3. The impregnated Bi/Al_2O_3 catalyst was prepared by a conventional impregnation method using an aqueous solution of $Bi(NO_3)_3 \cdot 3H_2O$, followed by drying at 373 K and calcination at 673 K for 2 h. The activation energies for the Bi/Al_2O_3 (11 wt %) (53 kJ mol^{-1}) and bulk Bi_2O_3 (57 kJ mol^{-1}) were similar to each other but much different from that

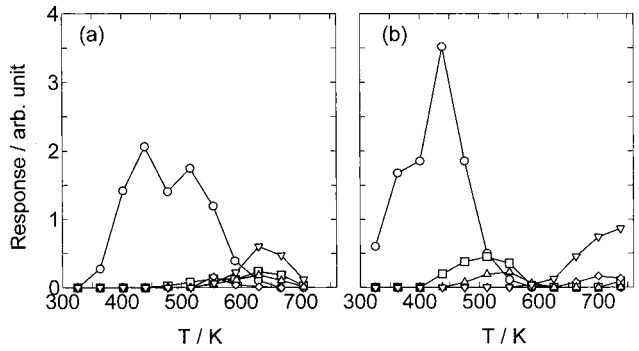

Figure 7. TPD spectra for adsorbed ethanol on (a) Bi/Al_2O_3 (3.0 wt %) and (b) Bi/Al_2O_3 (11.0 wt %). (○) C_2H_5OH, (□) CH_3CHO, (△) CH_3COOH, (▽) CO_2, and (◇) $C_2H_5OC_2H_5$.

for the 7.6 wt % Bi/Al_2O_3 catalyst (96 kJ mol^{-1}). The catalyst prepared by the impregnation method showed a much lower activity than that of the Bi/Al_2O_3 catalyst prepared by using $Bi(OEt)_3$. The activation energy (84 kJ mol^{-1}) was also different.

Figure 7 shows the TPD spectra of adsorbed ethanol on the 3.0 and 11.0 wt % loading Bi/Al_2O_3 catalysts. The main desorption product was ethanol, and small amounts of acetaldehyde, acetic acid, CO_2, and diethyl ether were also observed. A big difference in the amount and temperature of acetaldehyde desorption between the two loadings was observed. A substantial amount of acetaldehyde desorbed at 400−600 K on the 11.0 wt % Bi/Al_2O_3 catalyst, while on the 3.0 wt % Bi/Al_2O_3 catalyst, almost no acetaldehyde was evolved at these temperatures, and instead, CO_2 acetaldehyde and acetic acid desorbed at 600−700 K at the same time. No hydrogen was evolved during the TPD, while water formation was observed, though its amount was hard to analyze under the conditions. Acetaldehyde formation was observed in the TPD spectra of adsorbed ethanol on the Bi/Al_2O_3 (11.0 wt %) catalyst pre-evacuated at 673 K in the absence of gas-phase O_2. As a consequence, it is supported that ethanol oxidation reaction proceeds by using lattice oxygen in the 11 wt % Bi/Al_2O_3 catalyst. The feature of ethanol desorption was also different between the two catalysts. In the case of the 3.0 wt % catalyst, two peaks at 450 and 520 K were observed. The peak at 520 K was not observed for the 11.0 wt % catalyst. On the active 11.0 wt % Bi/Al_2O_3 catalyst, strongly adsorbed ethanol was not prevalent, and it was oxidized to acetaldehyde by the lattice oxygen atoms. The TPD results demonstrate that the difference in the catalytic activity between the 3.0 wt % Bi/Al_2O_3 catalyst and the 11.0 wt % Bi/Al_2O_3 catalyst is attributed to the amount and reactivity of the lattice oxygen atoms.

The kinetic data and the results of characterization indicate that the active species is the Bi (rich)−Al binary oxide clusters with a γ-Bi_2O_3-like structure, which are preferably produced in the high-loading (≥10 wt %) catalysts. The active catalysts have Bi−Bi bonds at 0.366 nm and longer Bi−O bonds at 0.277 nm. The activation energies for 11 wt % Bi/Al_2O_3 and bulk Bi_2O_3 were similar to each other, as described above. These results suggest that the active oxygen species is essentially the same as that for Bi_2O_3. On the contrary, the surface of the conventional impregnation Bi/Al_2O_3 catalyst seems to be similar to that of the 7.6 wt % Bi/Al_2O_3 catalyst with a much lower activity.

The present results demonstrate that the difference in activity is attributable to the difference in the local structure of active sites and that the reactivity of lattice oxygen is affected by the local structure around bismuth atom.

4. Conclusions

(1) We prepared bismuth oxide clusters at an Al_2O_3 surface by using $Bi(OEt)_3$ as a precursor, which showed the catalytic activity for the selective oxidation of ethanol.

(2) The active bismuth oxide clusters were not prepared by a conventional impregnation method using $Bi(NO_3)_3 \cdot 3H_2O$.

(3) The active clusters prepared above 9 wt % Bi loading were suggested to be Bi (rich)−Al binary oxides with γ-Bi_2O_3-like structure.

(4) The active binary-oxide clusters at the Al_2O_3 surface were obtained most efficiently when Bi loadings were 10−11 wt %.

(5) Below Bi loadings of 9 wt %, a Bi−Al (rich) binary-oxide monolayer was formed at the Al_2O_3 surface, which showed negligible activity.

(6) The activation energies for the catalytic ethanol oxidation on the Bi (rich)−Al binary-oxide clusters on Al_2O_3 and the Bi−Al (rich) binary-oxide monolayers on Al_2O_3 were 53 and 96 kJ mol^{-1}, respectively, which were roughly comparable to those for bulk Bi_2O_3 and the impregnation Bi/Al_2O_3 catalyst, respectively.

(7) The catalytic-selective oxidation proceeded by a redox mechanism via active lattice oxygen atoms.

(8) The catalytic activity was attributed not to the size of the oxide clusters but to the structure of binary oxides.

Acknowledgment. This work was supported by CREST (Core Research for Evolutionary Science and Technology) of Japan Science and Technology Corporation (JST). The XAFS measurements were taken with the approval of Photon Factory advisory committee (PAC) (Proposal 98G111).

References and Notes

(1) Iwasawa, Y. *Stud. Surf. Sci. Catal.* **1996**, *101*, 21.
(2) Iwasawa, Y. *J. Phys. IV* **1997**, *7*, C267.
(3) Iwasawa, Y. *Catal. Today* **1993**, *18*, 21.
(4) Iwasawa, Y. *Adv. Catal.* **1987**, *35*, 187.
(5) Mestl, G.; Srinivasan, T. K. K. *Catal. Rev.—Sci. Eng.* **1998**, *40*, 451.
(6) Dunn, J. P.; Stenger, H. G.; Wachs, I. E. *J. Catal.* **1999**, *181*, 233.
(7) Okumura, K.; Asakura, K.; Iwasawa, Y. *J. Phys. Chem. B* **1997**, *101*, 9984.
(8) Bond, G. C. *Appl. Catal., A* **1997**, *157*, 91.
(9) Centi, G. *Appl. Catal., A* **1996**, *147*, 267.
(10) Watling, T. C.; Deo, G.; Seshan, K.; Wachs, I. E.; Lercher, J. A. *Catal. Today* **1996**, *28*, 139.
(11) Asakura, K.; Inukai, J.; Iwasawa, Y. *J. Phys. Chem.* **1992**, *96*, 829.
(12) Castillo, R.; Koch, B.; Ruiz, P.; Delmon, B. *J. Catal.* **1996**, *161*, 524.
(13) Gao, X. T.; Bare, S. R.; Fierro, J. L. G.; Banares, M. A.; Wachs, I. E. *J. Phys. Chem. B* **1998**, *102*, 5653.
(14) Guliants, V. V. *Catal. Today* **1999**, *51*, 255.
(15) Prinetto, F.; Ghiotti, G.; Occhiuzzi, M.; Indovina, V. *J. Phys. Chem. B* **1998**, *102*, 10316.
(16) VanderVoort, P.; White, M. G.; Vansant, E. F. *Langmuir* **1998**, *14*, 106.
(17) Glinski, M. *Appl. Catal., A* **1997**, *164*, 205.
(18) Inumaru, K.; Misono, M.; Okuhara, T. *Appl. Catal., A* **1997**, *149*, 133.
(19) Kytokivi, A.; Jacobs, J. P.; Hakuli, A.; Merilainen, J.; Brongersma, H. H. *J. Catal.* **1996**, *162*, 190.
(20) Iwasawa, Y., Ed. *Tailored Metal Catalysts*; Reidel: Dordrecht, Holland, 1986.
(21) Ma, J.; Chuah, G. K.; Jaenicke, S.; Gopalakrishnan, R.; Tan, K. L. *Ber. Bunsen-Ges. Phys. Chem.* **1996**, *100*, 585.
(22) Molina, R.; Centeno, M. A.; Poncelet, G. *J. Phys. Chem. B* **1999**, *103*, 6036.
(23) Chu, H. P.; Lei, L. C.; Hu, X. J.; Yue, P. L. *Energy Fuels* **1998**, *12*, 1108.
(24) Okumura, K.; Iwasawa, Y. *J. Catal.* **1996**, *164*, 440.
(25) Shirai, M.; Asakura, K.; Iwasawa, Y. *J. Phys. Chem.* **1991**, *95*, 9999.
(26) Asakura, K.; Iwasawa, Y. *J. Phys. Chem.* **1991**, *95*, 1711.
(27) Engweiler, J.; Harf, J.; Baiker, A. *J. Catal.* **1996**, *159*, 259.

(28) Logie, V.; Maire, G.; Michel, D.; Vignes, J. L. *J. Catal.* **1999**, *188*, 90.
(29) Grasselli, R. K. *Catal. Today* **1999**, *49*, 141.
(30) Centi, G.; Trifiro, F. *Catal. Rev.—Sci. Eng.* **1986**, *28*, 165.
(31) Bettahar, M. M.; Costentin, G.; Savary, L.; Lavalley, J. C. *Appl. Catal., A* **1996**, *145*, 1.
(32) Carrazan, S. R. G.; Martin, C.; Rives, V.; Vidal, R. *Appl. Catal., A* **1996**, *135*, 95.
(33) MoroOka, Y.; Ueda, W. *Adv. Catal.* **1994**, *40*, 233.
(34) Zeng, Y.; Lin, Y. S. *Appl. Catal., A* **1997**, *159*, 101.
(35) Maple, M. B. *Bull. Mater. Res. Soc.* **1989**, *14*, 20.
(36) Stern, E. A.; Newville, M.; Ravel, B.; Yacoby, Y.; Haskel, D. *Phys. B* **1995**, *208*, 117.
(37) Stern, E. A. *Phys. Rev. B* **1993**, *48*, 9825.
(38) Ankudinov, A. L.; Ravel, B.; Rehr, J.; Conradson, S. D. *Phys. Rev. B* **1998**, *58*, 7565.
(39) Malmros, G. *Acta Chem. Scand.* **1970**, *24*, 384.
(40) Harwig, H. A. *Z. Anorg. Allg. Chem* **1978**, *44*, 151.